arXiv:1108.0006v1 [cond-mat.soft] 29 Jul 2011

Stress Response in Confined Arrays of Frictional and Frictionless Particles

Abdullah Cakir and Leonardo E. Silbert
Department of Physics, Southern Illinois University, Carbondale, Illinois 62901, USA

Stress transmission inside three dimensional granular packings is investigated using computer simulations. Localized force perturbation techniques are implemented for frictionless and frictional shallow, ordered, granular arrays confined by solid boundaries for a range of system sizes. Stress response profiles for frictional packings agree well with the predictions for the semi-infinite half plane of classical isotropic elasticity theory down to boxes of linear dimensions of approximately forty particle diameters and over several orders of magnitude in the applied force. The response profiles for frictionless packings exhibit a transitional regime to strongly anisotropic features with increasing box size. The differences between the nature of the stress response are shown to be characterized by very different particle displacement fields.

PACS numbers: 62.20.-x 81.70.Bt 83.80.Fg

I. INTRODUCTION

The manner in which granular materials respond to external loads belongs to a class of problems related to mechanical stability. Questions surrounding mechanical stability of particulate media have broad economical, environmental, and societal applications. These include the common practical problem of a collapsing grain silo, numerous natural events such as avalanches and mud slides, along with other unexpected destructive occurrences like dam breakage. Many such events are reported annually and readily convey the dramatic, and often catastrophic, effects that are primarily due to the failure of various granular systems.

The general physical theme that connects such a disparate range of problems is that of determining the underlying stress state of the system. Given information on the distribution of stresses within the system, can we predict whether such systems will remain mechanically stable, and what are the conditions that might promote or inhibit failure? One possibility is to employ established theories such as continuum, linear, elasticity theory [1]. Although elasticity theory applies over a wide range of situations, deviations from classical elasticity theory show up on a regular basis as some of the assumptions that underpin the theory break down. These problems have largely been emphasized over the past 15 years or so in studies of packings of granular materials. The essential point to note is that granularity, or the discreteness of the particles that constitute the packing, play a vital role in the resulting stress characteristics of the system due to a lack of a separation of length scales. Thus, it is becoming increasingly necessary to probe the relevant limits of classical elasticity theory and its range of valid application. For instance, classical elasticity is often assumed to remain valid not only at macroscopic scales to infer stress properties from displacement fields during loading events of the lithosphere [2], but also at the microscopic level of interrogation in studies of nanoscopic indentation in relation to physical metallurgy [3, 4].

A convenient method to test the range of validity of classical elasticity theory in granular systems that has been utilized over the past decade is the localized force perturbation technique. This procedure has the particular benefit that for an isotropic elastic material the stress profile in response to localized forcing - Green function response - can be determined without the need for any free parameters. We review this result for the case of three dimensions - Boussinesq equations - in the following section (and see the Appendix). To summarize efforts to date, studies on two- and three-dimensional granular packings indicate that disordered and frictional systems tend to follow the predictions of isotropic elasticity theory. Whereas, ordered packings composed of frictionless particles result in strongly anisotropic stress profiles that are not consistent with a linear, isotropic, elastic model. Such anisotropic profiles (see below for a more qualitative definition) have been debated in relation to anisotropic elasticity theory based on differential equations of the elliptic class [5], and alternative descriptions of the hyperbolic wave variety [6, 7]. To distinguish between the traditional isotropic result and anisotropic stress profiles we refer to these as *one-peak* and *two-peak* response profiles respectively, in reference to two dimensional experiments and simulations that have reported these observations [8–14].

In recent computer simulations the role of structure for frictionless granular packings on the stress response in a pseudo-infinite medium was investigated [15]. These studies showed that for ordered and quasi-ordered arrangements of frictionless grains, the response function was two-peak but consistent with the framework of an anisotropic elastic theory. A phenomenological model was employed to fit these anisotropic profiles that necessarily captured the two-peak character of the response profiles. As the structural disorder of the packing was increased, the stress response crossed over to a one-peak response, more in line with isotropic behavior.

The problem addressed here is to determine how confinement affects the stress response of granular packings. In most previous studies samples were used of sufficient size that the perturbed packings could be considered as semi-infinite in extent. In some cases the roughness of the

supporting base in packings prepared under gravity was seen to influence the magnitude of the stress response, although the response profiles retained isotropic, elastic character [16]. We also highlight two particularly relevant efforts that have been proposed to describe stress response specific to two dimensional systems. Extensions to three dimensions and especially for fully confined, shallow packings remains an ongoing effort. A non-linear elasticity formalism was developed [17] that captures the main features of experimental results for two dimensional granular packings [8]. The isotropic result is recovered through a multipole expansion of the normal stress response component σ_{zz} of classical elasticity. This theory was also able to describe anisotropic profiles by including generalized nonlinear strain components through the introduction of phenomenologically defined elastic constants. A future extension of this particular formalism may be useful in describing the stress response for a wide range of granular systems in both two and three dimensions. Additionally, force perturbation simulations of confined Lennard-Jones glasses [18] found a range of stress response profiles that appear, at least superficially, similar to some of the isotropic results we present here. Moreover, in some of the above examples a stress response crossover was reported either with system size and/or packing arrangement. This suggests that stress response investigations on granular packings can provide a route to understanding stress states in a range of systems where the discreteness of the constituent particles come into play.

However, there currently remains a distinct lack of a systematic study on the role that system size plays in modifying the stress response in granular materials. We propose that such a study is needed with the ever-growing emphasis on the design of small devices where the particulate nature of the material eventually dominate the system properties. Moreover, from this study we can estimate relevant length scales over which continuum elasticity theory remains valid, and below which alternative descriptions may be needed. Thus, our goal here is to provide a qualitative guide map to the typical system parameters for which classical elasticity theory is likely to apply and those for which more advanced techniques may be needed to predict their properties.

This paper is organized as follows. In the Section II we summarize the Boussinesq equations of classical, isotropic, linear elasticity theory for an infinite half-plane, and discuss other possibilities that predict anisotropic stress response profiles. In Section III we provide an overview of the computational technique and the packing preparation protocol implemented in this work. Section IV presents our main findings for the stress response behavior in frictional and frictionless particle packings. We end with conclusions and discussion.

II. BOUSSINESQ EQUATIONS

The equations of classical elasticity theory are derived from differential equations of the elliptic class that rely on the identification of well defined displacement fields of elements constituting the continuous elastic medium [19]. The analytical solutions for the problem of a localized point force applied vertically at the surface of an elastic, isotropic, infinite half-space are called the Boussinesq equations [1, 19]. In Cartesian coordinates, where the origin of the coordinate system coincides with the application point of the vertical force, $F_{\rm app}$, the components of the displacement fields are given by,

$$\begin{aligned} u_x &= \tfrac{F_{\rm app}}{4\pi G}\left[\tfrac{xz}{\rho^3} - (1-2\nu)\tfrac{x}{\rho(\rho+z)}\right] \\ u_y &= \tfrac{F_{\rm app}}{4\pi G}\left[\tfrac{yz}{\rho^3} - (1-2\nu)\tfrac{y}{\rho(\rho+z)}\right] \\ u_z &= \tfrac{F_{\rm app}}{4\pi G}\left[\tfrac{z^2}{\rho^3} + \tfrac{2(1-\nu)}{\rho}\right] \end{aligned} \tag{1}$$

where $\rho = \sqrt{x^2+y^2+z^2}$. Both G, the modulus of rigidity, and ν, the Poisson ratio, are material parameters characterizing the bulk properties of the elastic medium. Based on thermodynamic grounds [19], the Poisson ratio is constrained by, $-1 < \nu < 0.5$, in three dimensions. Through implementation of Hooke's law between stress and strain components, one then obtains expressions for components of the stress tensor. For the specific case when the force is applied in the 'downwards' or negative z-direction (see Fig. 1) the normal stress in the direction of the applied force, σ_{zz}, characterizes the response of the system. We focus primarily on this component of the stress although we also provide information on the normal stress components not in the direction of the applied force, σ_{xx} and σ_{yy}. We give expressions for all three normal stress components

$$\begin{aligned} \sigma_{xx} &= \tfrac{F_{\rm app}}{2\pi}\left[\tfrac{1-2\nu}{r^2}\left((1-\tfrac{z}{\rho})\tfrac{x^2-y^2}{r^2} + \tfrac{zy^2}{\rho^3}\right) - \tfrac{3zx^2}{\rho^5}\right] \\ \sigma_{yy} &= \tfrac{F_{\rm app}}{2\pi}\left[\tfrac{1-2\nu}{r^2}\left((1-\tfrac{z}{\rho})\tfrac{y^2-x^2}{r^2} + \tfrac{zx^2}{\rho^3}\right) - \tfrac{3zy^2}{\rho^5}\right] \\ \sigma_{zz} &= \tfrac{3F_{\rm app}}{2\pi}\tfrac{z^3}{\rho^5} \end{aligned} \tag{2}$$

where $r = \sqrt{x^2+y^2}$.

The stress response scales linearly with the applied force. Deviations from this indicate non-linear behavior, which, in the case of a particulate medium, corresponds to non-affine, or irreversible, particle displacements in response to the applied load. We reiterate that that there are no fitting parameters in σ_{zz} for the case of a semi-infinite half space. Therefore, we can quantify the influence of boundaries, or confinement, through a comparison of the Boussinesq result of Eq. 2, with our computed stress response for confined systems. Furthermore, we can also quantify deviations from isotropy from the stress profiles. We find that although the application of Boussinesq theory might at first seem to be inappropriate for

the systems investigated here, we find that for packings of sufficient linear size the classical theory captures the essential features of the stress properties and we classify the conditions for which isotropic elasticity theory are suitable.

III. SIMULATION METHODS

A. The Contact Forces and Equations of Motion

We implement a granular dynamics (GD) variant on molecular dynamics simulations [20] that has been designed to simulate granular systems [21]. Here we provide a summary of the technique [22]. For this particular study we focus on noncohesive, monodisperse sphere packings composed of elastic spheres of diameter d and mass m, that interact only on contact, through forces that act in directions that are normal $\mathbf{n}$, and tangential $\mathbf{t}$, to the contact plane, defined via

$$\begin{aligned} \mathbf{n} &= \frac{\mathbf{r}_{ij}}{r_{ij}} \\ \mathbf{t} &= \mathbf{1} - \mathbf{n} \end{aligned} \tag{3}$$

where $\mathbf{r}_{ij} = \mathbf{r}_i - \mathbf{r}_j$, is the separation between particles i and j, located at positions $\mathbf{r}_i$ and $\mathbf{r}_j$ respectively, and $r_{ij} = |\mathbf{r}_{ij}|$. $\mathbf{1}$ represents the unit vector.

The normal and tangential contact forces $F_{n,t}$ are based on a linear spring-dashpot model characterized by normal and tangential linear spring constants $k_{n,t}$, and damping factors $\gamma_{n,t}$, that account for elastic deformation of the contact point and inelasticity respectively,

$$\begin{aligned} F_n &= -k_n \delta_{ij} - m_{\text{eff}} \gamma_n v_{ij}^n \\ F_t &= -k_t s_{ij} - m_{\text{eff}} \gamma_t v_{ij}^t. \end{aligned} \tag{4}$$

Here, $\delta_{ij} \equiv (r_{ij} - d)$ is the surface compression of two particles undergoing a collision and $v_{ij}^{n,t}$ the relative normal/tangential velocity. The effective mass, $m_{\text{eff}} = m/2$, for the systems studied here. The quantity s_{ij} represents the integrated displacement of the contact point while two particles remain in contact. Friction is implemented through a local Coulomb yield criterion: $F_t \leq \mu F_n$, for a given friction coefficient μ. In this work, μ takes on the values zero and one. Thence, the total contact force is given by $\mathbf{F} = F_n \mathbf{n} + F_t \mathbf{t}$. Interactions between the particles and the walls are given by similar expressions where the wall is characterized by an effective mass of unity and the wall friction coefficient μ_W takes on the same values as that of the particles. The results are presented in simulation units. Length scales are given in units of d, timescales in units of $\sqrt{d/g}$, where g is the acceleration due to gravity, forces in units of mg, stresses in units of mg/d^2, and energies are given in units of mgd. Table I shows the simulation parameters used in this study. We point out that the values of the spring constants are fixed throughout this study resulting in a particle scale Poisson ratio of zero.

TABLE I: Physical parameters used in this simulation study. k_n and k_t are normal and tangential spring constants in units of mg/d. γ_n and γ_t are normal and tangential damping factors in units of $\sqrt{g/d}$. For values used here the particle Poisson ratio is zero. The particle friction coefficient is μ and the coefficient of inelasticity e.

Number of Particles	N	1000 - 100000
Normal Stiffness	k_n	$1 \times 10^5 mg/d$
Tangential Stiffness	k_t	$1 \times 10^5 mg/d$
Normal Damping Coefficient	γ_n	$50\sqrt{g/d}$
Tangential Damping Coefficient	γ_n	$\gamma_n/2$
Normal Restitution Coefficient	e	0.88
Particle Friction Coefficient	μ	0, 1.0
Wall Friction Coefficient	μ_W	0, 1.0

B. Coarse Graining Procedure

Stresses are computed from the contact forces. To enable an accurate determination of stresses from microscopic to macroscopic length scales, we follow the protocol developed by Goldhirsch and colleagues [23]. We implement a coarse graining procedure into the microscopic stress expression [24]. The coarse graining function chosen is a 3D Gaussian, and the resulting expression for the stress components at some location $\mathbf{r}$ is,

$$\sigma_{\alpha\beta}(\mathbf{r}) = \frac{1}{2} \sum_{i \neq j} F_{ij\alpha} r_{ij\beta} \int_0^1 ds \frac{1}{\pi^{3/2} \omega^3} e^{-(|\mathbf{r} - \mathbf{r}_i + s\mathbf{r}_{ij}|)^2/\omega^2}, \tag{5}$$

where ω is the coarse graining length scale. $\mathbf{F}_{ij}$ represents the force experienced by particle i in contact with particle j, obtained from Eq. 4. The numerical prefactor $(\sqrt{\pi}\omega)^{-3}$ is the normalization factor.

To implement Eq. 5 into our calculations we adopted a spatial grid over which to evaluate the coarse grained stress. To achieve sufficient spatial resolution we fixed the grid size $= 0.1d$ and $\omega = 1.0d$. (We computed stresses for a range of ω and grid sizes for our 3D systems and found that $0.5d < \omega < 5d$ provides a suitable plateau window [25], at an acceptable computational cost.)

C. Packing Generation Protocol

In this work we investigate how confinement influences the nature of stress response in granular packings. Because of the potentially large parameter space we fixed many features of the packings and focus our attention on a subset of variables. More specifically, we studied face centered cubic (FCC) ordered arrays of monodisperse spheres confined within a walled box. To prepare the initial configuration, we placed non overlapping particles at the lattice points of an FCC structure at the hard sphere packing fraction, $\phi_{\text{FCC}} = \pi/\sqrt{18}$. The packings are confined within open-top boxes, consisting of flat

side walls and a bottom base. We defined a coordinate system as shown in Fig. 1. The bottom plane of the box defines the xy-plane, while gravity points in the $-z$ direction. The size of the simulation boxes were chosen to be commensurate with the crystal structure. For the FCC structures the lattice unit is defined as $a = \sqrt{2}d$. Most of the results presented here are for boxes with square bases of side lengths, L, ranging from, $7a \approx 10d$ to $70a \approx 100d$. We also studied rectangular shaped boxes. The total number of particles N, was chosen by fixing the height, H, of all packings to be, $H \approx 10d$.

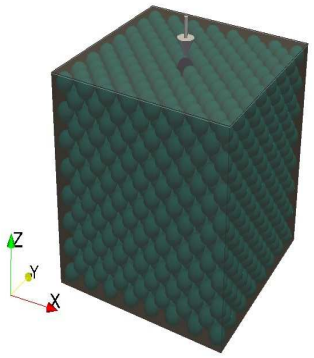

FIG. 1: A computer simulation snapshot of a typical system studied in this work. The packing is composed of monodisperse spheres arranged into a face centered cubic array, confined by 4 side walls, a solid base with an open top. The application of a localized perturbative force is represented by the arrow and the coordinate system is defined in the figure. $x = 0$ and $y = 0$ define the center of box in the bottom of box. Gravity points in the $-z$ direction.

After the particles were positioned at the lattice sites, we switched on gravity and allowed the particles to settle until the energy per particle, $E/N \approx 10^{-16}mgd$, reached numerical precision. This then defines our initial configuration. We recorded the positions of the particles, the contact forces between interacting particles, and consequently the stress, $\sigma_{\rm i}$, of this initial state. We then identified the top middle region of the packing, locating the particles in this region.

The second part of the simulation involves applying a downwards-pointing localized perturbation force, $F_{\rm app}$, to the top middle particle(s), and allowing the system to relax back to a mechanically stable state. We varied the magnitude of this applied force over several orders of magnitude, $0.01mg \leq F_{\rm app} \leq 100mg$, to check the limits of the linear regime. Again, we tracked particle positions and contact forces, and the final stress state $\sigma_{\rm f}$ [26]. The response function is calculated as the difference between the final and initial stress states, which we denote simply as,

$$\sigma \equiv \sigma_{\rm f} - \sigma_{\rm i}. \tag{6}$$

To make a clearer connection with previous experimental studies and visualizations [8, 27]. we present our results in a convenient format that can be readily compared with previous studies and theoretical predictions. In particular, we make use of three dimensional contour stress maps and two dimensional stress profiles which view the stress response in a given plane of the box or angularly-averaged slice across this plane, respectively. Given the box geometry that we employ, it is convenient to visualize $\sigma_{\rm zz}$ as a stress map in the horizontal plane. Using these plots it is relatively straightforward to distinguish between isotropic and anisotropic response profiles. These typically show up more clearly in stress profiles as single- and double-peak response profiles respectively. In all our stress maps lighter shading indicates larger stresses. We also present results on particle displacement fields taken in the plane.

IV. RESULTS

A. Frictional Packings

Our first results show that ordered arrays of *frictional* granular packings display isotropic elastic-like stress response behavior as seen in Fig. 2. These stress maps convey the "single-peak" nature of the stress response measured at the bottom of the packing for different system sizes for one value of the applied force, $F_{app} = 1mg$. Thus, we immediately note that the Boussinesq equation appears to describe confined systems. However, we find that system size and force magnitude influence this picture. We quantify the regime over which the classical expression remains suitably valid in two ways: Firstly, we compare our stress profiles to the Boussinesq expression and extract the full width at half maximum. Secondly, we identify the linear regime as a function of the applied force.

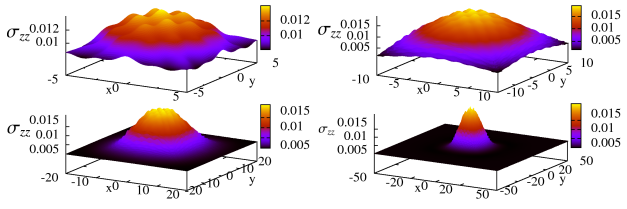

FIG. 2: Frictional systems $\mu = 1$. Stress response maps of σ_{zz} at the bottom boundary due to an applied force $F_{app} = 1mg$, for different system sizes, $10d \leq L \leq 100d$ indicated by scale in panels.

To cast this data into a more familiar form we circularly average the stress map data of Fig. 2 to construct stress profiles and directly compare with the predictions

of Eq. 2, from which we also obtain the full width of the response peaks. In Fig. 3(a) we show our averaged response profiles for systems of different height, clearly indicating a single-peak response consistent with the classical theory shown by the thick solid line. We note that

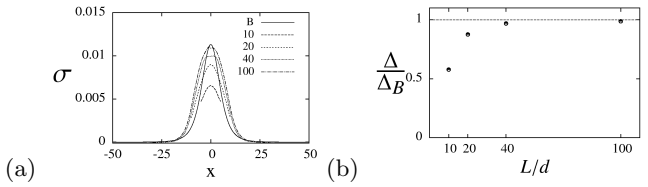

FIG. 3: (a) Averaged stress response profiles, σ, for one value of the applied force $F_{app} = 1mg$ for systems of fixed height $H \approx 10d$ and varying side lengths $L = 10d$ (long dash line), $20d$ (thin solid line), $40d$ (dashed), $100d$ (dotted), and B (solid line), the Boussinesq result. (b) Δ full width at half height of the stress profiles for the simulation data (symbols) relative to the theoretical result Δ_B. Perfect agreement indicated by dashed line.

for the smallest system ($L = 10d$) the stress profiles do not accurately conform to the Boussinesq form. To better quantify deviations from Eq. 2 we extract the full width at half height, Δ, and compare with the theoretical result $\Delta_B = 1.113H$, shown in Fig. 3(b). We find that for $L > 40d$, the single-peak response profiles are suitably described by Eq. 2, with better agreement for larger system size as expected.

Thus, we have identified a minimum system size for which the classical expression describes the data accurately, $L \gtrsim 40d$. To further test our results with Eq. 2, we again fit the data and now allow the applied force parameter in Eq. 2 to vary as a fitting parameter, denoted here as F_B, which we then compared to the actual force applied during the simulation, F_{app}. Our results shown in Fig. 4 clearly indicate that confined systems of box sizes greater than $L \gtrsim 40d$ conform to the semi-infinite system size result.

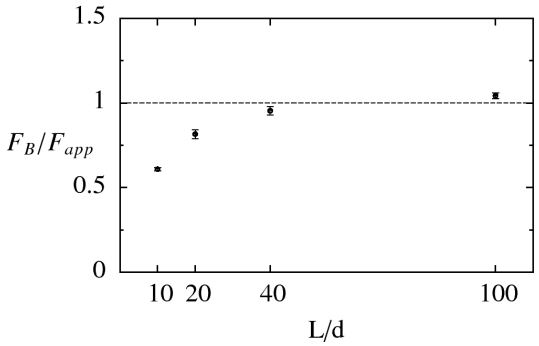

FIG. 4: Comparison between the actual applied force $F_{app} = 1mg$ versus F_B, the fitted force using the Boussinesq equation, Eq. 2, to fit the stress profile data at the bottom of a frictional granular packing for boxes of different sizes, with side lengths $10d \le L \le 100d$. Perfect agreement indicated by dashed line.

The magnitude of the applied force also strongly influences the response function. For small applied forces, the stress response remains isotropic consistent with the classical result as seen in the previous figures. Beyond some force threshold the stress response becomes anisotropic due to the FCC arrangement of the grains and Eq. 2 is no longer valid as indicated by the stress maps in Fig. 5. To quantify this effect and identify the linear regime as a function of applied force, we performed a similar analysis as described above. We varied the applied force over several orders of magnitude, $0.01mg \le F_{app} \le 100mg$, applied to a system size of side length $L = 40d$. Figure 6 shows that the fitted force increases linearly with applied force with unit slope when the magnitude of the perturbation force remains below $F_{app} \simeq 60mg$. In ongoing work to be reported elsewhere [28] we find that this threshold also depends on the friction coefficient. Thus,

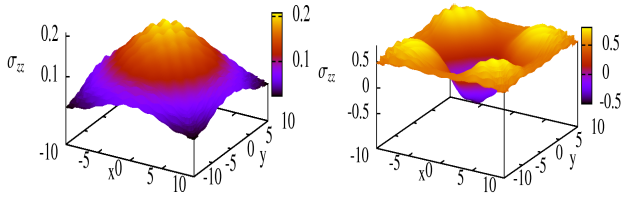

FIG. 5: Stress response map, σ_{zz}, for the bottom of the box of a frictional system of size $L = 20d$, Left panel: $F_{app} = 10mg$. Right panel: $F_{app} = 100mg$.

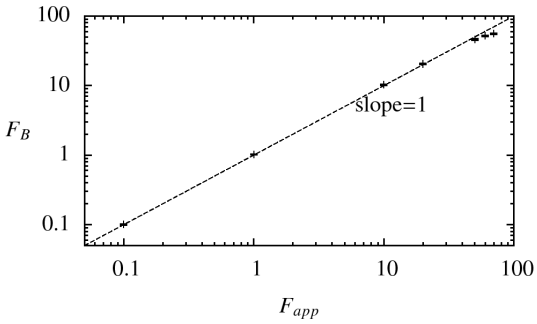

FIG. 6: Comparison between the actual applied force F_{app} versus F_B, the fitted force using the Boussinesq equation to fit the stress profile data at the bottom of a frictional granular packing of side length $L = 20d$.

in summary, we find that for ordered frictional packings the stress state is suitably described by the semi-infinite result even for relatively small systems over a wide range in applied forcing and we have quantified the linear regime over which this agreement exists.

In an effort to investigate the underlying mechanisms responsible for the changing character of the stress response in our different systems we have computed the normal stress response at different distances from the source of the force perturbation which are shown in Fig. 7. The left hand panels in Fig. 7 show data for our smallest system, $L = 10d$, which deviates strongly from the classical predictions despite appearing to retain

a single broad peak response profile. While the right hand columns are for a larger system, $L = 40d$, that is consistent with the Boussinesq expression. As expected at the top of packing (top panels) the stress is localized at the point of perturbation. Deeper into the packings the stress response broadens. For the smallest system the stress quickly spreads across the entire region of the packing while for larger systems the stress peak remains relatively localized within the central region of the packing.

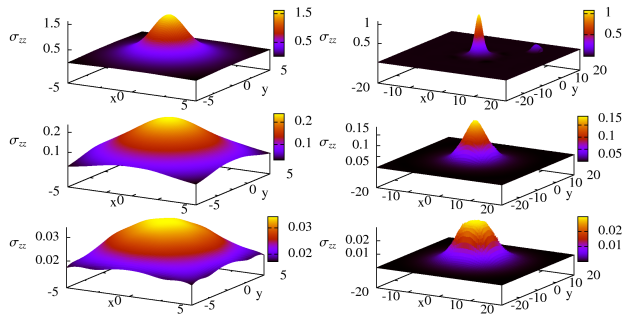

FIG. 7: Stress maps, σ_{zz}, in response to a localized force of magnitude $F_{app} = 1mg$ applied at the top of the packing. The panels show data at different distances from the perturbation source. Rows show data for layer 1 (top), 3, and 8 (near bottom), for $L = 10d$ (left column panels) and $L = 40d$ (right column panels).

The reason behind this changing stress response is a strong reflective component of stress from the side walls as the stress is transmitted away from the source of the perturbation. To qualify this effect, in Fig. 8 we plot the averaged normal stresses, $\frac{1}{2}(\sigma_{xx} + \sigma_{yy}) =$ "σ_{xx}", exerted at the side walls for our different systems, and data for the classical expression using a value of the Poisson ratio of $\nu = 0.4$. Indeed, we find that for the smaller systems the stress at the side walls is much larger than that expected from the classical behavior of side wall stress from Boussinesq equation and the corresponding larger system size. To generate the data presented in Fig. 8 it is necessary to introduce the material Poisson ratio ν. Our final choice for ν was made on the best fit between the stress profiles obtained via the displacement fields, Eq. 1, and the displacement fields constructed from the simulation data. We matched our simulation displacement fields for our largest system to the predictions of Eq. 1 using ν as a fitting parameter. Our confined packings therefore behave as a continuum material with an effective Poisson ratio, $\nu \approx 0.4$. This procedure actually provides a convenient method to determine material properties of composite materials such as granular packings [29]. The benefit of analyzing the displacement fields is that we can view the direct microscopic response of the system at the particle scale due to the imposed localized force perturbation.

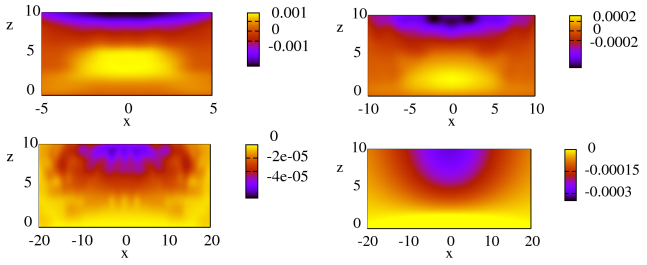

FIG. 8: Normal stress, σ_{xx}, at the side wall for frictional packings of height $\approx 10d$ and side length, $L = 10d$, $20d$, $40d$ and the classical expression for a system of size $L = 40d$ (bottom right panel), using $\nu = 0.4$.

The displacement fields of the middle vertical slice for frictional packings of different size are plotted in Fig. 9. We also include a comparison to Eq. 1 for a system of size $L = 100$, using $\nu = 0.4$. These changes in the displacement fields of the perturbed system result in a larger reflection of stress at the side walls hence causing deviations in the overall stress response of smaller systems compared with the semi-infinite size result. However, it is worth pointing out that these differences occur only for relatively small packings of size $L \lesssim 20d$. Above this size, these frictional packings appear to be suitably described by the Boussinesq formalism.

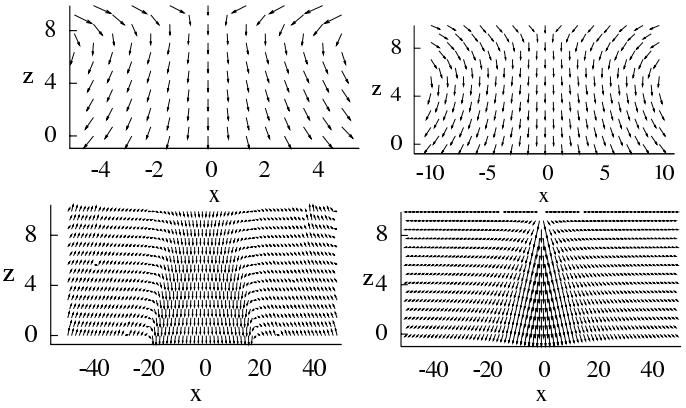

FIG. 9: Displacement field vectors in the vertical plane for a central slice inside packings of side length $L = 10, 20, 100d$, and the result of Eq. 1 on a system of size $L = 100d$, using $\nu = 0.4$.

B. Frictionless Packings

In contrast to frictional packings, *frictionless* ordered arrays display primarily strongly anisotropic stress behavior in response to localized force perturbations. In Fig. 10 the stress component σ_{zz} for frictionless arrays of different sizes are compared. Apart from the smallest system size, the response profiles are ringed or multi-peaked with a minimum in the stress response characteristic of an anisotropic response function in clear contrast to the frictional packings of Fig. 2. Surprisingly, however, the smallest system of size $L = 10d$ exhibits a stress response that initially appears isotropic in nature - a maximum in

the stress in the middle of the packing - but with some unusual features not seen in the frictional case. In fact this smaller system does not conform to the Boussinesq stress profile even though an isotropic-like single peak response is observed.

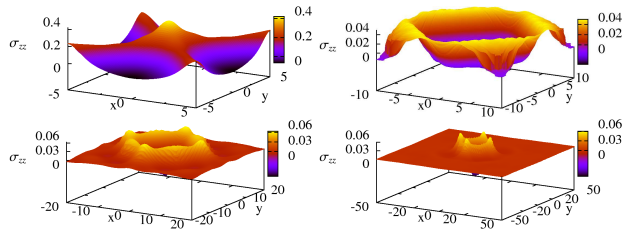

FIG. 10: Frictionless systems $\mu = 0$. Stress response maps of σ_{zz} at the bottom boundary due to an applied force $F_{app} = 1mg$, for different systems sizes, $10d \leq L \leq 100d$.

The influence of confinement plays a significant role in modifying the stress properties for frictionless packings even within the same packing. To investigate this effect further, stress response maps at different distances from the source of the force perturbation are shown in Fig. 11 for two system sizes, $L = 10d, 40d$. In the vicinity of the localized force perturbation, the stress response also takes on localized features where the stress is concentrated in a region directly below the point of application. At intermediate distances between the top and bottom of the packing both systems now display strongly anisotropic stress profiles with a stress minimum focused in the region beneath the point of force application. However, as noted above, the response measured at the bottom of the packing dramatically changes character between the two system sizes. These features suggest that the stress state of small frictionless packings can not only vary substantially within the packing, but exhibit highly unusual stress properties compared to both larger frictionless systems and frictional packings.

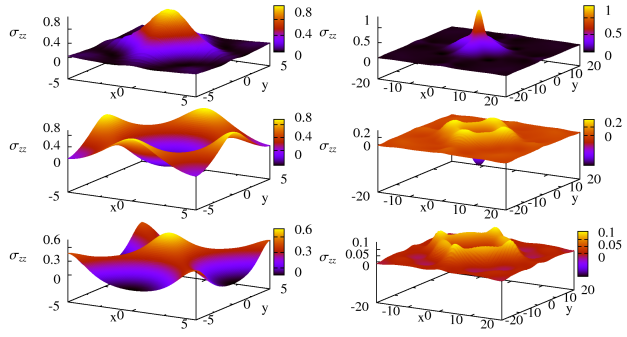

FIG. 11: Stress maps, σ_{zz}, in response to a localized force of magnitude $F_{app} = 1mg$ applied at the top of the packing. The panels show data at different distances from the perturbation source. Rows show data for layer 1 (top), 3, and 8 (near bottom), for $L = 10d$ (left column panels) and $L = 40d$ (right column panels).

Again we find that these unusual stress properties are a direct result of the manner in which stresses are transmitted and interact with the side wall boundaries due to the strongly correlated displacement fields of the particles during the response process. Visualization of the displacement fields for these frictionless packings are particularly illuminating as shown in Fig. 12. These displacement vectors are taken from a middle slice inside the different packings. For the smallest packing (top left panel in Fig. 12), the particle displacements in response to the applied perturbation show a directional structure that is responsible for the increased stress reflection at the side walls. Interestingly, this reflection shields the bottom of the packing from the growing stress minimum apparent at intermediate depths. Whereas, for larger systems the stress response is seen to be dominated by particle displacements along directed rays through the system responsible for the anisotropic profiles observed at the bottom of the packings.

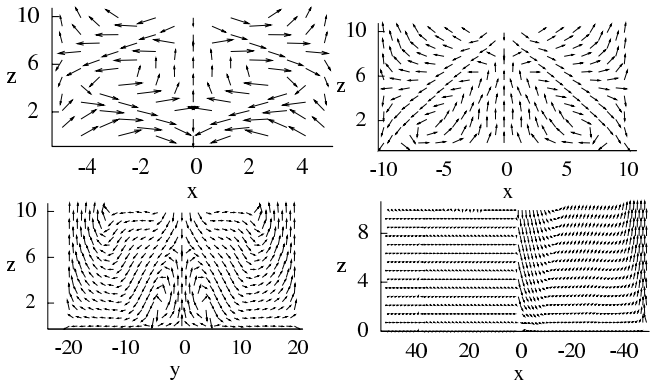

FIG. 12: Displacement field vectors in the vertical plane for a central slice inside packings of side length $L = 10, 20, 40, 100d$.

The results presented above suggest that there exists some crossover response for confined, frictionless packings that depends on the size of the system. We have investigated the changing character of the stress response and its dependence on box size. This crossover behavior is illustrated in stress response maps of Fig. 13, where the box side lengths have been incrementally increased from $L = 12d - 18d$. It is apparent that changing box size results in large-scale stress fluctuations that span the system as the stress response crosses over from a more isotropic-like response (smaller systems) to strongly

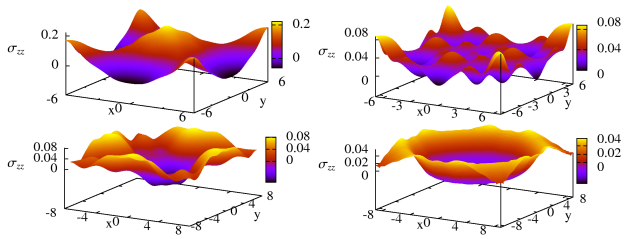

FIG. 13: Crossover behavior of the stress response, σ_{zz}, with increasing box size for systems of side length, $12d \leq L \leq 18d$.

anisotropic behavior (larger system). There is a region of box sizes for these frictionless packings where the stress state of the system exhibits peculiar behavior that does not conform to either a pseudo-isotropic description nor can it be considered anisotropic in character. These features can have implications in the design of mechanical systems at small scales where confinement can have a large effect on the stress state of the system.

We have also investigated the role of box geometry on the nature of the stress response. As shown earlier we find that for the smaller frictionless systems confined within a square-base box with $L_x = L_y = 10d$, the stress response exhibits a broad peak in the central region of the base. We find that highly unusual and complex features emerge if we now increase the size of only one side of the box into a rectangular base keeping $L_x = 10d$ fixed. Stress maps for this scenario are shown in Fig. 14, where we have increased the side ratio from 1 to 10. These result emphasize the importance of box size and geometry on the nature of stress response in shallow packings.

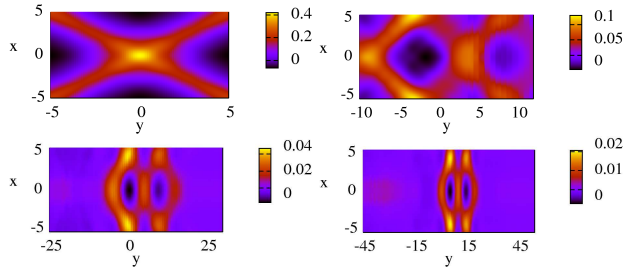

FIG. 14: Evolution of the stress response, σ_{zz}, in frictionless packings as one side of the confining box is increased from a square base of side lengths $L_x = L_y = 10d$, to a rectangular base of side lengths $L_x = 10d$ and $L_y = 23d$, $L_x = 10d$ and $L_y = 50d$, $L_x = 10d$ and $L_y = 100d$.

V. CONCLUSIONS

Using computer simulations of a model granular material, we have studied the nature of the stress response in shallow and confined granular crystalline arrays. Packings composed of highly frictional particles generally exhibit a stress response function measured at the bottom of the packing that resembles that of an isotropic, elastic material that is well described by the Boussinesq equations of classical elasticity. Thus, the semi-infinite half-space result remains suitably valid to describe the stress state of the system provided the size of the base of the confining walls is larger than approximately 40 particle diameters. In this regime the stress response appears to behave as a linear elastic material. For smaller frictional systems, the stress response exhibits confinement effects that are not accurately captured by the classical result. Packing arrangement and the influence of the boundaries have significant effects on the stress state of the system. Furthermore, due to the FCC crystalline arrangements studied here, anisotropic stress response behavior is observed at large applied forces whereby the influence of structure starts to dominate the stress properties.

Frictionless packings exhibit stress response properties that are generally anisotropic in nature due to the FCC arrays. However, smaller packings can be tuned to observe a range of behaviors depending on the location within the packing for square boxes, or on the ratio of the side lengths for rectangular systems. Complex response patterns emerge for frictionless rectangular arrays. We also point out that for the anisotropic profiles - either with zero friction or for large forcing - the resulting stress response indicates a decrease in the stress relative to the initial state prior to perturbation, i.e. in the measures defined here the stress becomes negative. This suggests that such force perturbations actually weaken the material relative to the unperturbed state.

Our results further suggest that there exists a transition in the underlying character of the response as the friction coefficient is varied. To highlight this possibility, we show in Fig. 15, the averaged stress profiles for a square-base, $L = 100d$, for different particle friction coefficients in response to an applied force, $F_{app} = 1mg$. Indeed we find that increasing the friction coefficient suppresses the stress dip in the central region of the packing until a single-peak response is recovered for moderate to large friction coefficients. We expect that the precise location of this transition will also depend on the magnitude of the applied force [28].

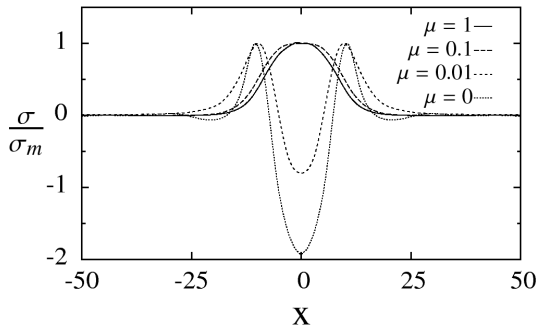

FIG. 15: σ, averaged stress profiles for different friction coefficients, μ, for one system size, $L = 100d$, in response to an applied force $F_{app} = 1mg$. Each stress profile is scaled by its maximum value, σ_m

Our studies indicate that for confined granular arrays, particle properties, magnitude of forcing, and geometry of the confining container can all be used to design materials with specific stress states. Through this accessible parameter space, confined granular packings can be made to mimic the properties of linear, isotropic, elastic materials, where the stress is concentrated beneath the point of perturbation - single-peak response. Or they can be designed to exhibit strongly anisotropic properties where stresses are transmitted along preferred directions. Moreover, for particular box geometries, the stress response can be transmitted approximately uniformly through the

system. Thus, it might be necessary to take into account the possible stress states indicated here during the design of microscopic granular devices and components.

VI. APPENDIX

Here we provide a short derivation of the normal stress response component σ_{zz} (see Eq. 2), within the framework of linear elasticity, indicating how the material parameters, G and ν, cancel from the expression given in Eq. 2. This derivation follows directly from Landau and Lifshitz [19]. The basic ingredient is the implementation of a constitutive relation between stress and strain that corresponds to Hooke's law: the normal stress σ_{zz} is linearly proportional to the strain components u_{xx}, u_{yy}, and u_{zz},

$$\sigma_{zz} = \frac{2G}{1-2\nu}\left[u_{zz} + \nu(u_{xx} + u_{yy} - u_{zz})\right] \qquad (7)$$

where the strain components are obtained from derivatives of the components of the displacement fields leading to

$$\begin{aligned} u_{xx} &= \tfrac{1}{4\pi G}\left[\tfrac{z}{\rho^3} - \tfrac{3x^2 z}{\rho^5} - \tfrac{1-2\nu}{\rho^2+\rho z} - \tfrac{(1-2\nu)x^2(2+\frac{z}{\rho})}{(\rho^2+\rho z)^2}\right], \\ u_{yy} &= \tfrac{1}{4\pi G}\left[\tfrac{z}{\rho^3} - \tfrac{3y^2 z}{\rho^5} - \tfrac{1-2\nu}{\rho^2+\rho z} - \tfrac{(1-2\nu)y^2(2+\frac{z}{\rho})}{(\rho^2+\rho z)^2}\right], \qquad (8) \\ u_{zz} &= \tfrac{1}{4\pi G}\left[\tfrac{2\nu z}{\rho^3} - \tfrac{3z^3}{\rho^5}\right], \end{aligned}$$

and we have set the value of the applied, perturbing force to unity for notational convenience.

Combining the above equations we find,

$$\sigma_{zz} = \frac{2G}{1-2\nu}\frac{1}{4\pi G}[\frac{2\nu z}{\rho^3} - \frac{3z^3}{\rho^5} + \nu(\frac{2z}{\rho^3} - \frac{3(x^2+y^2)z}{\rho^5} - \frac{2(1-2\nu)}{\rho^2+\rho z} - \frac{(1-2\nu)(x^2+y^2)(2+\frac{z}{\rho})}{(\rho^2+\rho z)^2} - \frac{2\nu z}{\rho^3} + \frac{3z^3}{\rho^5}]$$

explicitly emphasizing the cancellation of G from the equation.

The resulting expression can be written as

$$\sigma_{zz} = \frac{1}{2\pi(1-2\nu)}[\frac{\nu z}{\rho^3}(4-2\nu-3) + \frac{z^3}{\rho^5}(3\nu+3\nu-3) - \frac{2\nu(1-2\nu)}{\rho^2+\rho z} - \frac{\nu(1-2\nu)(1-\frac{z}{\rho})(2+\frac{z}{\rho})}{\rho^2+\rho z}]$$

and with further algebra,

$$\sigma_{zz} = \frac{1}{2\pi}\left[\frac{\nu z}{\rho^3} - \frac{3z^3}{\rho^5} - \frac{1}{\rho^2+rz}(2\nu - 2\nu + \frac{\nu z}{\rho} + \frac{\nu z^2}{\rho^2})\right]$$

The terms containing ν cancel out and one obtains Eq. 2 for an arbitrary applied force, $F_{\rm app}$, directed in the $-z$ direction.

VII. ACKNOWLEDGEMENTS

This work is dedicated to Isaac Goldhirsch. We acknowledge support from the National Science Foundation CBET-0828359.

[1] K. L. Johnson, *Contact Mechanics* (Cambridge University Press, Cambridge, 1987).
[2] J. M. Becker and M. Bevis, Geophysical Journal International **156**, 171 (2004).
[3] O. V. Semenova, I. A. Zashivalova, and O. A. Morozov, Technical Physics Letters **34**, 601 (2008).
[4] J. Menčík, Meccanica **42**, 19 (2007).
[5] M. Otto, J. P. Bouchaud, P. Claudin, and J. E. S. Socolar, Phys. Rev. E **67**, 031302 (2003).
[6] J. P. Bouchaud, M. E. Cates, and P. Claudin, J. Phys. I France **5**, 639 (1995).
[7] J. P. Wittmer, M. E. Cates, and P. Claudin, J. Phys. I France **7**, 39 (1997).
[8] J. Geng, D. Howell, E. Longhi, R. P. Behringer, G. Reydellet, L. Vanel, E. Clément, and S. Luding, Phys. Rev. Lett. **87**, 035506 (2001).
[9] M. Muthuswamy and A. Tordesillas, Journal of Statistical Mechanics: Theory and Experiment **2006**, P09003 (2006).
[10] C. Goldenberg and I. Goldhirsch, Phys. Rev. E **77**, 041303 (2008).
[11] J. Ai, J. Chen, J. Rotter, and J. Ooi, Granular Matter **13**, 133 (2011).
[12] E. H. B. Amar, D. Clamond, N. Fraysse, and J. Rajchenbach, Phys. Rev. E **83**, 021304 (2011).
[13] K. Liffman, M. Nguyen, G. Metcalfe, and P. Cleary, Granular Matter **3**, 165 (2001).
[14] C. Goldenberg and I. Goldhirsch, Nature **435**, 188 (2005).
[15] L. E. Silbert, Granular Matter **12**, 135 (2010).
[16] D. Serero, G. Reydellet, P. Claudin, E. Clément, and D. Levine, The European Physical Journal E: Soft Matter and Biological Physics **6**, 169 (2001).
[17] B. P. Tighe and J. E. S. Socolar, Phys. Rev. E **77**, 031303 (2008).
[18] F. Leonforte, A. Tanguy, J. P. Wittmer, and J. L. Barrat, Phys. Rev. B **70**, 014203 (2004).
[19] L. D. Landau and E. M. Lifshitz, *Theory of Elasticity* (Elsevier, Oxford, 1986).
[20] M. P. Allen and D. J. Tildesley, *Computer simulation of liquids* (Clarendon Press, New York, NY, USA, 1989).
[21] S. J. Plimpton, J. Comput. Phys. **117**, 1 (1995), URL

http://lammps.sandia.gov.
[22] L. E. Silbert, *Experimental and Computational Techniques in Soft Condensed Matter Physics* (CUP, New York, 2010), chap. 5, ed. J. Olafsen.
[23] I. Goldhirsch, Granular Matter **12**, 239 (2010).
[24] C. Goldenberg and I. Goldhirsch, Phys. Rev. Lett. **89**, 084302 (2002).
[25] C. Goldenberg, A. P. F. Atman, P. Claudin, G. Combe, and I. Goldhirsch, Phys. Rev. Lett. **96**, 168001 (2006).
[26] The coarse graining function is integrated over all space then normalized to the value of the applied force F_{app}.
[27] G. Reydellet and E. Clément, Phys. Rev. Lett. **86**, 3308 (2001).
[28] L. E. Silbert and A. Cakir (2011), unpublished.
[29] W. G. Ellenbroek, M. van Hecke, and W. van Saarloos, Phys. Rev. E **80**, 061307 (2009).